BIN1/Amphiphysin 2 and ezrin drive filopodia-like structures in myoblasts

Laura Picas, Franck Comunale, Charlotte André-Arpin, Hugo Bousquet, Feng-Ching Tsai, Félix Rico, Paolo Maiuri, Julien Pernier, Stéphane Bodin, Anne-Sophie Nicot, et al.

BIN1/Amphiphysin 2 and ezrin drive filopodia-like structures in myoblasts

Laura Picas[1*], Franck Comunale[2], Charlotte André-Arpin[1], Hugo Bousquet[3], Feng-Ching Tsai[4], Félix Rico[5], Paolo Maiuri[6], Julien Pernier[7], Stéphane Bodin[2], Anne-Sophie Nicot[8], Jocelyn Laporte[9], Patricia Bassereau[4], Bruno Goud[3], Cécile Gauthier-Rouvière[2#*], Stéphanie Miserey[3#*].

[1]Institut de Recherche en Infectiologie de Montpellier (IRIM), CNRS UMR 9004, University of Montpellier, Route de Mende, Montpellier, France.

[2]CRBM, University of Montpellier, CNRS, Montpellier, France.

[3]Institut Curie, PSL Research University, CNRS UMR 144, Paris, France.

[4]Institut Curie, PSL Research University, CNRS UMR 168, Paris, France.

[5] U1067 INSERM, Aix-Marseille Université, Marseille, France.

[6]FIRC (Italian Foundation for Cancer Research) Institute of Molecular Oncology (IFOM), Milan, Italy.

[7]Université Paris-Saclay, CEA, CNRS, Institute for Integrative Biology of the Cell (I2BC), Gif-sur-Yvette, France.

[8]Grenoble Alpes University, Inserm, U1216, Grenoble Institut Neurosciences, Grenoble, France.

[9]Department of Translational Medicine, IGBMC, U1258, UMR7104, Strasbourg University, Collège de France, Illkirch, France.

[*] Corresponding authors

[#] equal contribution

Abstract

Amphiphysin 2 (BIN1) is a membrane and actin remodeling protein mutated both in congenital and adult centronuclear myopathies. The BIN1 muscle-specific isoform finely tunes muscle regeneration in adulthood and regulates myoblast fusion. However, the underlying molecular mechanisms are unknown. Here, we report that BIN1 is required for myoblast fusion and participates in the formation of filopodia-like structures at myoblast intercellular junctions. BIN1 bundles actin *in vitro* and regulates the membrane-to-cortex attachment, two key processes required for myoblast fusion. We identified ezrin, a member of the ERM protein family, as a new BIN1 partner and showed that BIN1 promotes ezrin association to $PI(4,5)P_2$ at the cell cortex. Our results establish BIN1 and ezrin as central players at the early stages of myoblast fusion to form long-lived filopodia-like structures.

Introduction

The membrane remodeling protein BIN1 (BIN1/amphiphysin-2) is ubiquitously expressed but enriched in muscle tissue and the brain. Notably, several BIN1 mutations are associated with centronuclear myopathies (CNMs), a heterogeneous group of inherited muscular disorders that are characterized by fiber atrophy and muscle weakness (Nicot et al., 2007; Fugier et al., 2011). *BIN1* gene displays 20 exons and encodes multiple isoforms (Prokic et al., 2014). Skeletal muscles express both an ubiquitous isoform that contains an N-terminal BAR domain -which recognizes and induces membrane curvature- and a C-terminal SH3 domain -involved in proline-rich domains interactions- and a muscle-specific isoform (BIN1 isoform 8 called BIN1 hereafter) that contains the in-frame exon 11 encoding a polybasic motif binding phosphoinositides (PIs). Ubiquitous BIN1 (isoform 9) is necessary for muscle development and function at birth and controls T-tubule formation and organelle positioning (Lee et al., 2002; D'Alessandro et al., 2015; Prokic et al., 2020). In contrast, BIN1 isoform 8 appears dispensable for muscle development but is required for muscle regeneration at adulthood (Prokic et al., 2020). BIN1 was shown to regulate the fusion of myoblasts *in cellulo* (Wechsler-Reya et al., 1998) and *in vivo* (Lee et al., 2002; Fernando et al., 2009; Prokic et al., 2020), but the molecular mechanisms are not well understood.

The actin cytoskeleton is the main driving force for myoblast fusion (Chen, 2011; Abmayr and Pavlath, 2012). Indeed, dense F-actin structures at the fusion site promote the formation of protrusions allowing cell membrane juxtaposition that provides the mechanical forces required to undergo cell-cell fusion (Sens et al., 2010; Kim et al., 2015). The formation of actin-based filopodia-like structures, also called fingers, at the fusion site was reported both in mammalian and *Drosophila* muscle cells (Abramovici and Gee, 2007; Sens et al., 2010; Shilagardi et al., 2013; Segal et al., 2016; Randrianarison-Huetz et al., 2018). These filopodia-like structures are dynamically controlled by Arp2/3-mediated branched actin polymerization and dynamin-mediated F-actin bundling (Sens et al., 2010; Shin et al., 2014a; b; Chuang et al., 2019; Zhang et al., 2020b).

BAR domain proteins are determinants of membrane curvature and contain domains allowing targeting to specific lipids and proteins. These characteristics make each member of the BAR family functionally distinct and determine its specific localization in the cell (Simunovic et al., 2016). BIN1 displays a PI-binding motif

responsible for its targeting to the plasma membrane, mainly by interacting with phosphatidylinositol 4,5-bisphosphate ($PI(4,5)P_2$) (Lee et al., 2002; Picas et al., 2014). The PI domain controls a conformational switch through the binding of the SH3 domain of BIN1. Hence $PI(4,5)P_2$ levels regulate BIN1 SH3 domain interaction with BIN1 partners such as dynamin (Kojima et al., 2004; Royer et al., 2013) or the neuronal Wiskott-Aldrich syndrome (N-WASP) protein that regulates actin polymerization through the Arp2/3 complex (Yamada et al., 2009; Falcone et al., 2014; D'Alessandro et al., 2015). BIN1 was proposed to integrate membrane curvature and actin dynamics. *In vitro* and *in cellulo* approaches have shown that BIN1 is associated with F-actin mainly through its BAR domain (D'Alessandro et al., 2015; Dräger et al., 2017). However, how BIN1 interacts and remodels the actin cytoskeleton during myoblast fusion is poorly understood.

Here, we report that BIN1 is required for myoblast fusion and participates in forming filopodia-like structures at myoblasts' intercellular junctions. Our results show that BIN1 assembles actin bundles *in vitro* and regulates plasma membrane tension, two key processes required for myoblast fusion. We identified ezrin as a new BIN1 partner and showed that ezrin association to $PI(4,5)P_2$-containing model membranes and the plasma membrane is favored by BIN1. Thus, we propose that BIN1-ezrin mediates the formation of long-lived filopodia-like structures favoring early stages of myoblast fusion.

Results

BIN1 promotes the formation of filopodia-like structures at intercellular junctions

To investigate the role of BIN1 in myoblast fusion, we generated stable C2C12 myoblast cell lines expressing specific short interfering RNA (shRNA) against *Bin1* or luciferase (CTRL shRNA). In undifferentiated *Bin1* shRNA C2C12 cells, depletion of BIN1 expression is almost complete (Fig. 1A). As reported, BIN1 expression increased during differentiation (Lee et al., 2002; Nicot et al., 2007), and we observed that the inhibition of BIN1 expression remained effective during the early stages of proliferation/differentiation of C2C12 cells (Fig. S1A).

BIN1 knock-down was previously shown to inhibit myotube formation (Wechsler-Reya et al., 1998; Lee et al., 2002). We confirmed this effect (Fig. S1B-C), and observed a decrease in the size of myotubes and the number of nuclei per myotube after 72h culture in the differentiation medium (Fig. S1A-C). We then performed a detailed analysis of the cellular morphology of control and C2C12 *Bin1* shRNA myoblasts by scanning electron microscopy (SEM) either under proliferative conditions and at 80-90% confluence to favor the formation of cell-cell junctions preceding myoblast fusion. BIN1 depletion was associated with a reduction of membrane extensions between cells and smoother dorsal plasma membrane (Fig. 1B and Fig. S1D). This phenotype was evident at the cell periphery and cell-cell junctions, indicating that BIN1 might participate in adjoining myoblasts' intercellular zippering. Conversely, we observed a dense interface of filopodia-like membrane protrusions interconnecting two or more adjacent myoblasts in control cells. In BIN1 knock-down cells, the protrusion densities are significantly decreased (3.6-fold reduction in filopodia-like structure density and a 2.2-fold increase in the filopodia-like structure length, Fig. 1C). These results show that in myoblasts, BIN1 depletion affects the morphology and the number of filopodia-like structure at cell-cell junctions and at the cell periphery (i.e., away from intercellular junctions).

Next, we determined the ability of BIN1, and the role of its functional domains (N-terminus BAR domain (N-BAR) and the C-terminus SH3 domain), in the formation of filopodia-like structure in C2C12 cells (Fig. 1D). GFP, GFP-BIN1 or GFP-tagged D151N and K575X BIN1 mutants were co-expressed with Lifeact-mCherry to monitor actin-rich extension density and average length. The D151N or the K575X BIN1 mutants are associated with the autosomal recessive form of centronuclear myopathies (Nicot et al., 2007; Royer et al., 2013). The BIN1 D151N mutant carries a mutation in

the N-BAR domain impairing membrane deformation (Wu et al., 2014), and the BIN1 K575X mutant displays a truncated SH3 domain shown to prevent its interaction with cellular effectors such as dynamin (Nicot et al., 2007) or N-WASP (Falcone et al., 2014). Expression of GFP-BIN1 in C2C12 cells increased filopodia-like structures density and average length, as compared to control conditions (GFP alone) (Fig. 1E-G). This increase was not observed upon expression of the D151N and K575X BIN1 mutants, suggesting that both the N-BAR and the SH3 domains of BIN1 regulate filopodia-like structure formation in C2C12 cells.

Altogether, these data show that BIN1 promotes formation of filopodia-like structures at intercellular junctions and that both its N-BAR and SH3 domains are required.

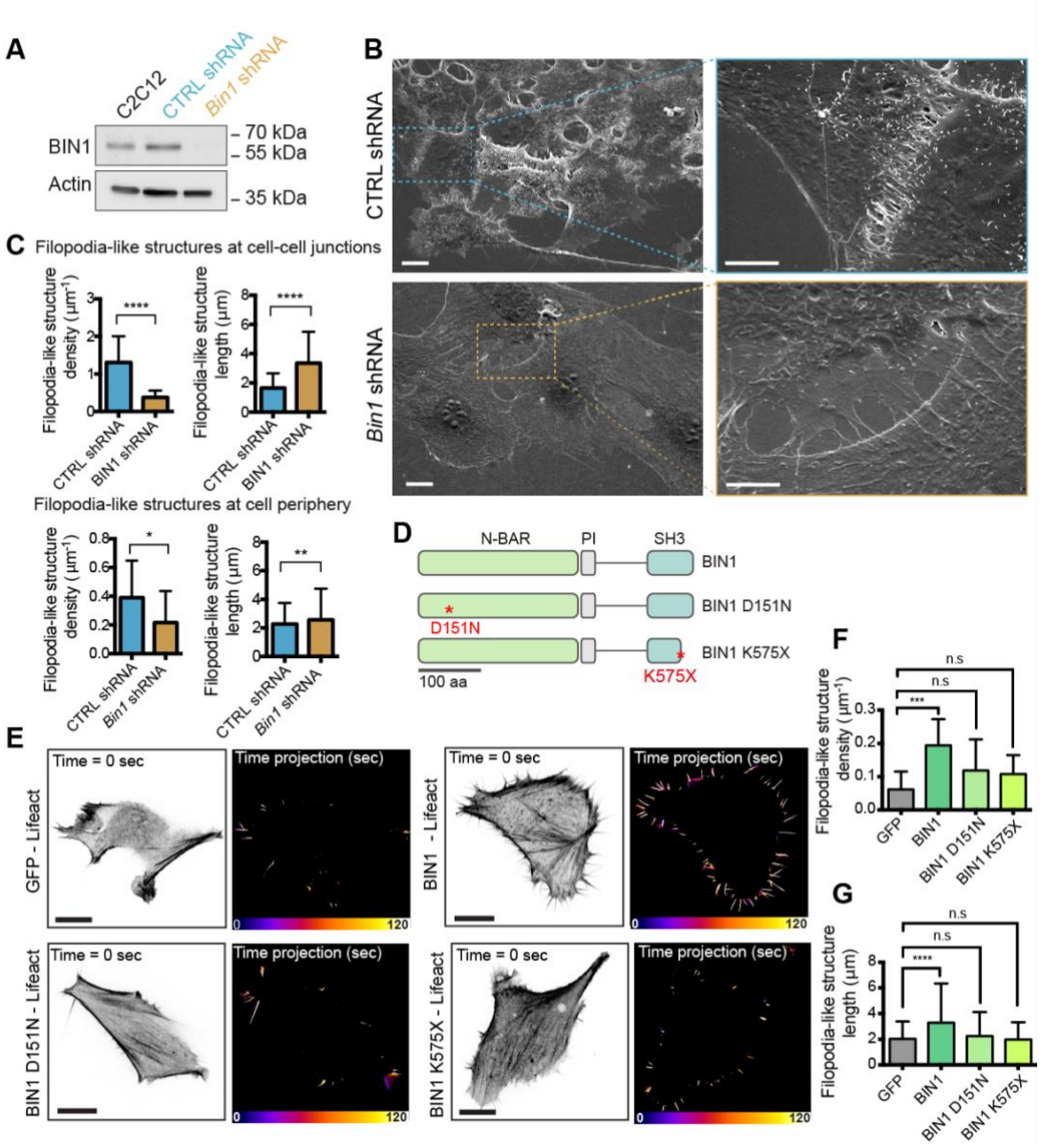

Figure 1. The N-BAR and SH3 domain are required for BIN1-mediated formation of filopodia-like structures

A) Western-blot analysis of the endogenous expression of actin and BIN1 on parental, CTRL shRNA (i.e. Luciferase) and BIN1 shRNA stable C2C12 myoblast cell lines. **B**) Representative scanning electron microscopy images of CTRL shRNA and BIN1 shRNA stable C2C12 myoblasts cultured in growth factor-containing medium. Scale bar, 10 µm and 5 µm for the magnified images. **C)** Quantification of the number and length of filopodia-like structures per cell at the cell periphery and at intercellular junctions measured from the SEM images. Cells: *N*=27, 38, 25 and 19 for the measure of filopodia density at cell-cell junctions and at the cell periphery of CTRL and BIN1 shRNA, respectively. n=666, 569, 851 and 391 for the measure of filopodia-like structure length at cell-cell junctions and at the cell periphery of CTRL and BIN1 shRNA cells, respectively. **D**) Domain representation (N-BAR, phosphoinositide-binding motif, PI, and SH3 domains) of BIN1 full-length. Stars highlight the D151N mutant at the N-BAR and the stop codon of the BIN1 K575X mutant. **E)** Representative still images of the actin signal (inverted LUT) obtained from spinning disk life cell imaging at t = 0 and time projection of the filopodia-like structure tracks (500 msec exposure, during 60s. Total time acquisition = 120s) of C2C12 cells co-transfected with mCherry-Lifeact and either GFP, GFP-BIN1, GFP-BIN1 D151N or GFP-BIN1 K575X. Only Lifeact is displayed in the images. Scale bar, 10 µm. Fire LUT color scale is 120s. **F**) Quantification of F-actin-rich filopodia-like structure density; *n*=11, 12, 12 and 12 for GFP, BIN1, D151N and K575X. n = number of cells from live cell imaging experiments. **G**) Filopodia-like structure length; *n*=80, 316, 159 and 144 for GFP, BIN1, D151N and K575X. n = number of filopodia-like structures. Error bars represent s.d.; ANOVA test: n.s > 0.1, * P < 0.1, ** P < 0.01, *** P < 0.001, **** P < 0.0001.

BIN1 associates with filamentous actin at filopodia-like structures

PI(4,5)P_2 is key for the recruitment of many actin regulatory proteins promoting actin polymerization and filopodia formation at the plasma membrane (Senju et al., 2017; Senju and Lappalainen, 2019), and we have previously shown that BIN1 clusters PI(4,5)P_2 to recruit its downstream partners (Picas et al., 2014). Accordingly, we confirmed that filopodia-like structures positive for BIN1 are highly enriched in PI(4,5)P_2 and F-actin (Fig. S2A). We thus investigated if BIN1 can impact actin organization in myoblasts. First, the co-localization of endogenous BIN1 with filamentous actin structures at filopodia was analyzed using immunofluorescence in C2C12 cells (Fig. 2A). As previously reported, BIN1 associates with the plasma membrane (Lee et al., 2002). We found that BIN1 is also present in filopodia-like structures protruding out of C2C12 cells (see ROIs in Fig. 2A). A detailed analysis of the co-localization of BIN1 with F-actin in filopodia-like structures was then performed using structured illumination microscopy (SIM) imaging in C2C12 cells expressing GFP-BIN1 and co-stained for F-actin (Fig. 2B). We observed that BIN1 is localized at the base of filopodia-like structures and displays a discontinuous labeling along these structures (Fig. 2B and Fig. S2A). This organization is different from that observed for fascin, another filopodia-associated protein reported to participate in the elongation and

bundling of filopodial actin filaments (Vignjevic et al., 2006), which appears homogenously localized all over filopodia (Fig. S2A).

To determine whether BIN1 localization in filopodia-like structures is related to its association with actin, we performed co-immunoprecipitation experiments using several GFP-tagged amphiphysin isoforms: amphiphysin-1 (typically associated to clathrin-coated membranes) (McMahon and Boucrot, 2011), N-amphiphysin-2 (BIN1 isoform 1, expressed in neurons and lacking the exon 11) and BIN1 (BIN1 isoform 8 called BIN1 hereafter) (Prokic et al., 2014) (Fig. 2C). These different amphiphysin isoforms were reported to bind actin *in vitro* (D'Alessandro et al., 2015; Dräger et al., 2017) and display strong homology in their N-BAR and SH3 domains. Immuno-blotting showed that *in cellulo,* only BIN1 is associated with actin. In addition, using an *in vitro* assay with purified actin and BIN1, we showed that full-length BIN1 can bundle actin filaments (Fig. 2D). Remarkably, this effect is dependent on BIN1 concentration. Indeed, the number of actin bundles increases with increasing BIN1 concentration, although we already observed a bundling effect at 0.1 μM of BIN1 with 1 μM of actin, as compared to other BIN1 isoforms (Dräger et al., 2017) (Fig. 2D).

Next, we established the contribution of the N-BAR and SH3 domains of BIN1 to its association with actin. The interaction of GFP-tagged BIN1, BIN1 D151N or BIN1 K575X mutants with actin was tested using co-immunoprecipitation experiments (Fig. 2E). Wild type (WT) BIN1 and both mutants associate with actin *in cellulo*. Detailed analysis of multi-color life-cell movies of C2C12 cells co-expressing Lifeact-mCherry and wild-type or mutated forms of BIN confirmed that all BIN1 forms are found co-localized with actin in filopodia-like actin filaments and that this co-localization is dynamic (Fig. 2F and Fig. S2B). Indeed, kymograph analysis of the GFP-BIN1 signal at the cell periphery showed that it often precedes that of Lifeact-mCherry (blue arrowheads, Fig. 2F). Moreover, BIN1 signal is present during the initiation, extension and retraction of filopodial actin filaments (Fig. 2F). The detailed quantification of the movies showed that BIN1 expression leads to a ~ 2-fold increase in the filopodia-like structure lifetime (i.e., time until the filopodia-like structure collapses), an effect that was also observed, although to a lesser extent (i.e. ~ 1.5-fold increase), after expression of the two BIN1 mutants (Fig. 2G). Importantly, the formation of BIN1-mediated filopodia-like structures requires the inverted-BAR (I-BAR) protein IRSp53 (Fig. 2H-J), a protein involved in the Cdc42-dependent formation

of filopodia-like protrusions made of actin bundles (Scita et al., 2008; Lim et al., 2008; Disanza et al., 2013). Collectively, our results show that whereas BIN1 and its mutated variants associate with F-actin in filopodia-like structures (Fig. 2E-F and Fig. S2A), only the WT BIN1 has an impact on their density (Fig. 1F), possibly through an IRSp53-based actin regulatory complex (Fig. 2I-J). Thus, in addition to the actin-binding and actin-remodeling abilities of BIN1, other interactions through the N-BAR and SH3 domains might participate in the regulation of BIN1-mediated filopodia-like structure formation and dynamics at the cell cortex.

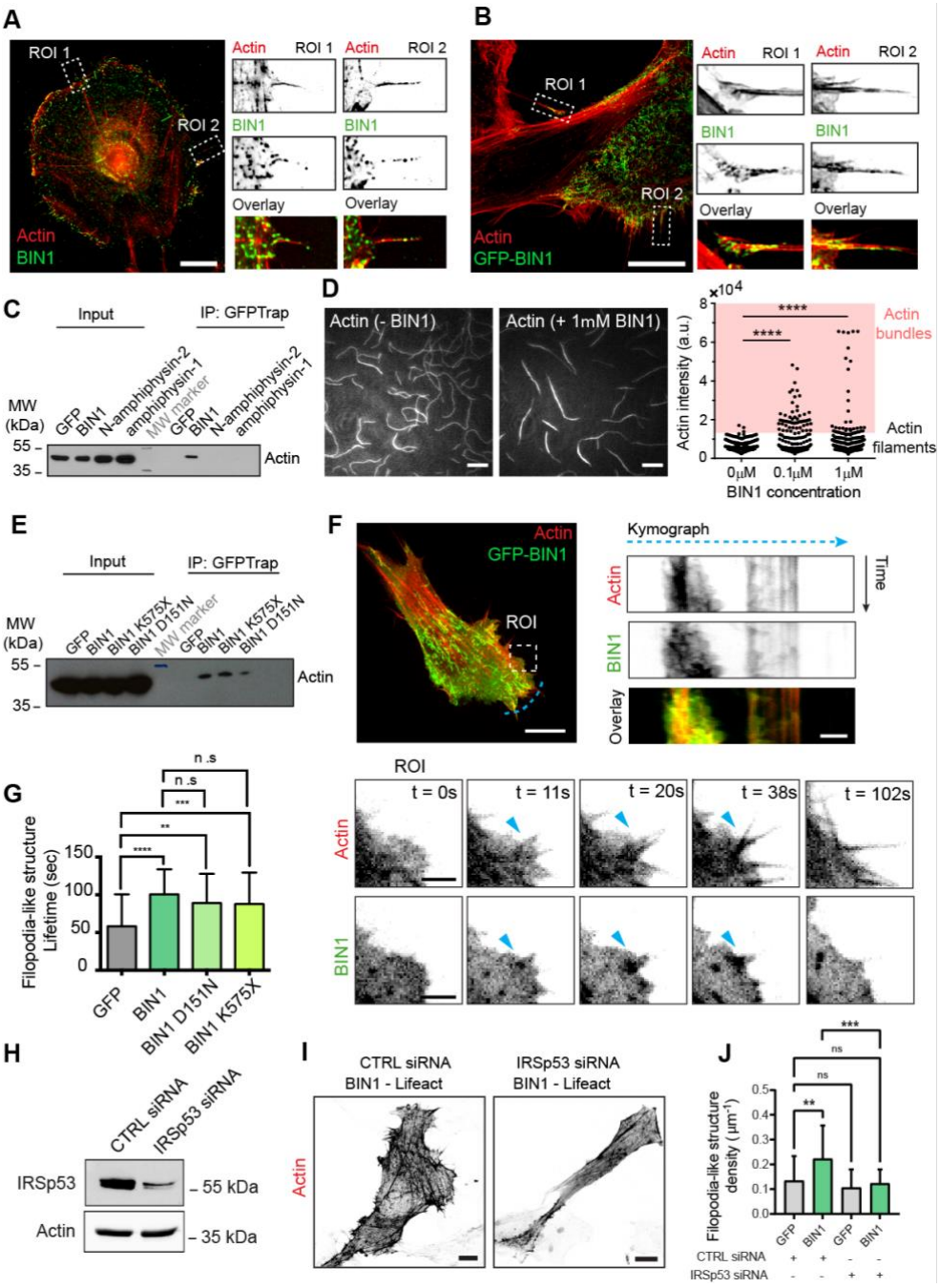

Figure 2. BIN1 interacts with F-actin *in vitro* and *in cellulo* at all stages of filopodia-like structure formation. **A)** C2C12 myoblasts stained for endogenous BIN1 (C99D antibody, green) and F-actin (phalloidin, red). Magnified images of two representative regions of interest (ROI). Scale bar, 10 µm. **B)** SIM images of C2C12 myoblasts expressing GFP-BIN1 (green) stained for F-actin (phalloidin, red) and magnified images of two representative ROIs in the corresponding image. Scale bar, 10 µm. **C)** GFP pull-downs using extracts from HeLa cells expressing either GFP, or GFP-BIN1, GFP-N-amphiphysin-2 and GFP-amphiphysin-1. Actin was detected by western blotting. HeLa cells were used to provide an unbiased cellular context. IP = immunoprecipitate. **D)** *In vitro* assay with purified actin and BIN1. TIRF images showing pre-polymerized F-actin filaments in the absence (- BIN1) or in the presence of BIN1 (+ 1 µM BIN1) and the corresponding quantification of the BIN1 bundling activity as denoted by the actin intensity in each condition. **E)** GFP-Trap pull-downs using extracts from C2C12 myoblasts expressing either GFP alone or fused with BIN1, BIN1 K575X or BIN1 D151N. Actin was revealed by western blotting. **F)** Top, representative spinning disk life cell imaging (500 msec exposure, during 60s. Total time acquisition = 120s) of C2C12 myoblasts co-transfected with Lifeact-mCherry and GFP-BIN1 at t = 0s. Kymograph analysis along the blue dashed line in the corresponding image at t = 0s, highlight the recruitment and binding of BIN1 to filopodia-like structures. Scale bar, 10 µm. Scale bar in kymograph and ROI, 2 µm. Bottom, representative time-lapse snapshots from the ROI region showing the localization of BIN1 on F-actin during filopodia-like structure formation in C2C12 cells, as highlighted by the blue arrowheads **G**) Filopodia lifetime; *n*=253, 1743, 711 and 785 for GFP, BIN1, D151N and K575X. **H)** Western-blot analysis of the endogenous expression of actin and IRSp53 on CTRL siRNA (i.e. Luciferase) and IRSp53 siRNA C2C12 cells. **I)** Representative z-projected confocal images showing the actin organization of CTRL siRNA and IRSp53 siRNA C2C12 cells co-transfected with GFP-BIN1 and Lifeact-mCherry. Only Lifeact is displayed in the images. J) Quantification of filopodia-like structure density; *n*=22, 26, 26 and 27 for CTRL siRNA and IRSp53 siRNA C2C12 cells co-transfected with either GFP or GFP-BIN1 and Lifeact-mCherry respectively. Error bars represent s.d.; ANOVA test: n.s > 0.1, ** P < 0.01, *** P < 0.001.

BIN1 and ezrin associate at filopodia-like structures in myoblast

To further understand the role of BIN1 in filopodia-like structure formation, we performed a proteomic analysis using GFP-BIN1 to identify new BIN1 partners (Fig. S3A). We validated already known BIN1 partners: dynamin 1 and 2 (Lee et al., 2002; Nicot et al., 2007) and actin (this study and D'Alessandro et al., 2015). Interestingly, we identified ezrin, a protein of the ezrin-radixin-moesin (ERM) family involved in the control of cell cortex mechanics (Diz-Muñoz et al., 2010; Zhang et al., 2020a) (Fig. S3A). ERM proteins display two conformational states: a cytosolic closed-conformation, which results from the intramolecular interaction of the N-terminal FERM domain with the C-terminal ERM-associated domain (C-ERMAD), and a membrane-bound opened-conformation, which requires a sequential activation through the interaction with $PI(4,5)P_2$, the subsequent phosphorylation of a conserved threonine in the actin-binding site of the C-ERMAD (T567, in ezrin) and finally, the interaction of the C-ERMAD with F-actin (Fievet et al., 2004). We decided to focus on BIN1/ezrin

interaction because ezrin was recently suggested to be involved in myoblast fusion (Zhang et al., 2022).

To validate BIN1/ezrin interaction specificity, we performed co-immunoprecipitation experiments using BIN1, amphiphysin-1 and N-amphiphysin-2 (Fig. 3A). Our results confirmed that only BIN1 associates with ezrin *in cellulo*. Moreover, only the BIN1 D151N mutant, but not K575X, associates with ezrin (Fig. 3B), suggesting that the C-terminal domain of BIN1 is required for the interaction with ezrin.

We then tested BIN1 and ezrin distribution during filopodia-like structure formation. We performed multi-color time-lapse live-cell imaging of C2C12 cells co-expressing mCherry-ezrin WT, which reports both the non-phosphorylated and active phosphorylated form of ezrin, together with either GFP-BIN1 WT or mutants. Representative still spinning-disk images showed that BIN1 and ezrin co-localize at the cell periphery (Fig. 3C-D). Detailed analysis of the dynamics of ezrin and BIN1 also showed that both proteins co-localized during filopodia-like structure formation (Fig. 3D-E) In addition, co-expression of ezrin with BIN1 potentiated the formation of filopodia-like structures compared to BIN1 alone (Fig. 3F), suggesting that BIN1 and ezrin might cooperate in this process. Conversely, no co-localization was observed between ezrin and the BIN1 mutants that do not induce the formation of filopodia-like structures (Fig. S3B), indicating that BIN1-ezrin mediated filopodia-like structure formation might require the coordinated contribution of the N-BAR and SH3 domains of BIN1.

Next, we analyzed the co-localization of the active phosphorylated form of endogenous ezrin (phospho-ezrin) with endogenous BIN1 in proliferating C2C12 cells at the time of myoblast fusion, where BIN1-mediated filopodia-like structures are observed (Fig. 1B). Under proliferative conditions (i.e. $\leq$ 90% cell confluency in growth medium) and at the onset of myoblast fusion (i.e. 24h after addition of differentiation medium), we observed high BIN1 expression associated with phospho-ezrin at the cell cortex (Fig. 3G) and on filopodia structures (as shown by the representative magnification in Fig. 3H). Collectively, the above data indicate that BIN1 and phospho-ezrin co-localized at filopodia-like structures and interact to promote their formation.

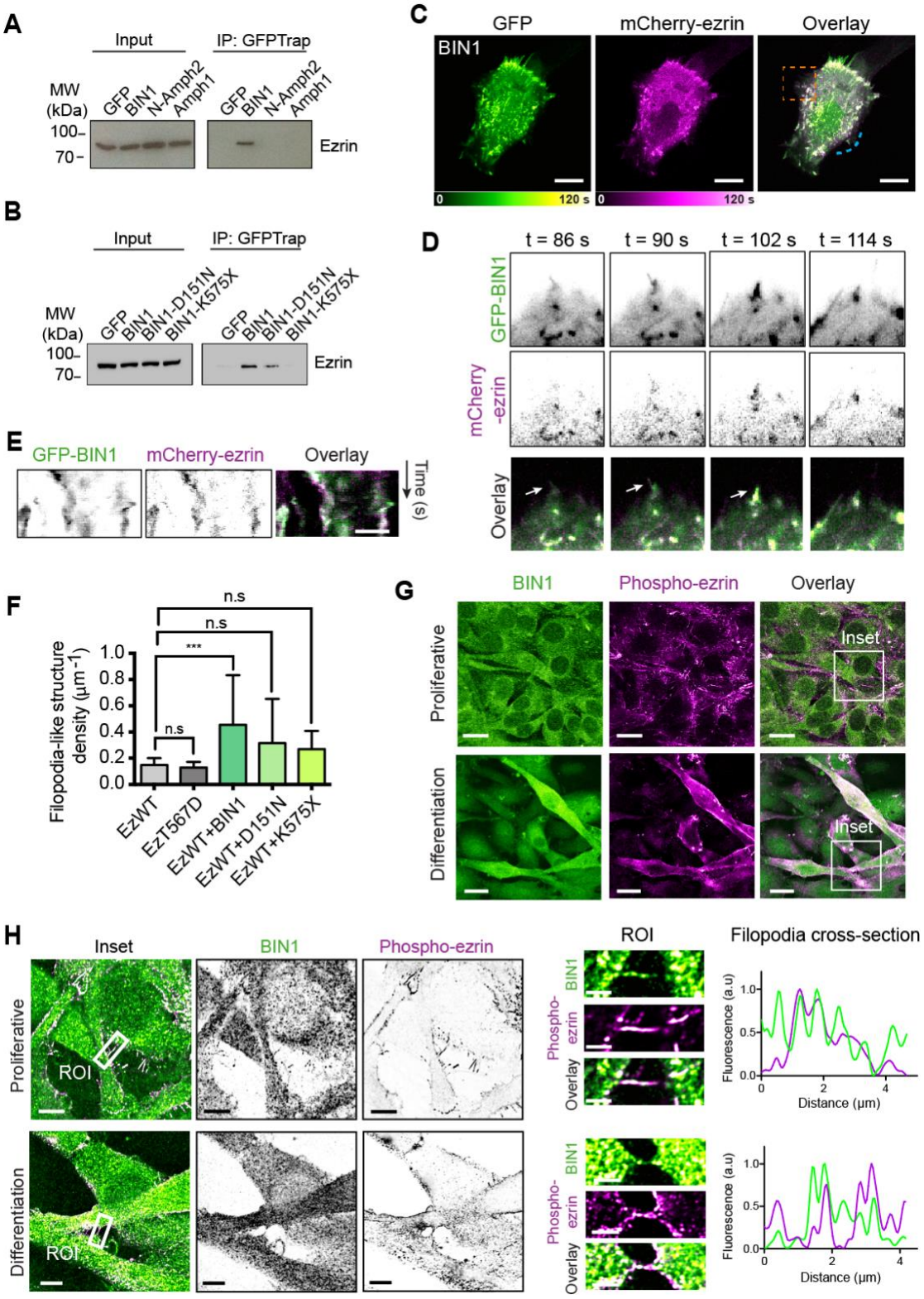

Figure 3. BIN1 associates to ezrin and co-localizes with ezrin in filopodia-like structures

A) GFP-Trap pull-downs from extracts of HeLa cells transfected with plasmids encoding GFP, GFP-BIN1, N-amphiphysin-2, or amphiphysin-1. Ezrin was revealed by western-blotting. **B)** GFP-Trap pull-downs using extracts from C2C12 myoblasts expressing either GFP alone or fused with BIN1, BIN1 K575X or BIN1 D151N. Ezrin was revealed by western-blotting. **C)** Representative time projection of spinning disk movies (500 msec exposure, during

60s. Total time acquisition = 120s) of C2C12 cells co-expressing mCherry-ezrin (magenta) and GFP-BIN1 (green). Scale bar, 10 μm. **D)** Representative time-lapse snapshots from the orange inset in D highlighting the co-localization of BIN1 and ezrin during filopodia-like structure formation (white arrows). **E)** Kymograph analysis along the blue dashed line in D. Scale bar in kymographs, 1 μm. **F**) Quantification of filopodia-like structure density; *n*=19, 17, 11, 10, and 10 for EzWT, EzT567D, BIN1, D151N and K575X, respectively. n = number of cells from live cell imaging experiments. Error bars represent s.d.; ANOVA test: n.s > 0.1, *** P < 0.001. **G)** Representative maximum intensity projected confocal images of proliferative myoblasts or at the onset of myoblast fusion (differentiation) stained for endogenous BIN1 (C99D antibody, green) and phosphorylated ezrin (phospho-ezrin, magenta). Scale bar, 20 μm. **H)** High magnification airyscan images of the inset in G. Images are maximum intensity projections of z = 2. Cross-section along a representative filopodia-like structure (BIN1 in green, phospho-ezrin in magenta) highlighted by the white box and magnified in the ROI image. Scale bar is 5 μm, and 2 μm for the inset.

BIN1 tunes ezrin recruitment at the cell cortex and regulates membrane-to-cortex association

To understand how BIN1/ezrin can cooperate in filopodia formation, we next investigated the impact of BIN1 knock-down on ezrin and phospho-ezrin expression and localization. Interestingly, we observed a 2-fold increase of phosphorylated ezrin in BIN1 knock-down C2C12 cells without modification in the total pool of ezrin (Fig. 4A). In addition, we observed that phospho-ezrin appears enriched at filopodia-like structures in control C2C12 cells (Fig. 4B). Such enrichment was not observed in C2C12 BIN1 shRNA myoblasts (Fig. 4B). These results indicate that although the total level of phospho-ezrin is increased in BIN1 knock-down myoblasts, phospho-ezrin is not observed at the cell cortex nor at filopodia-like structures. This observation reflects that ezrin requires BIN1 to associate with the plasma membrane and suggests that the known $PI(4,5)P_2$ clustering effect of BIN1, as we previously reported (Picas et al., 2014), might play a role to facilitate ezrin recruitment.

Next, using an *in vitro* reconstituted system consisting of supported lipid bilayers doped with 5% $PI(4,5)P_2$, we quantified the binding of recombinant wild type ezrin and its phospho-mimetic form (T567D) (Gautreau et al., 2000; Shabardina et al., 2016) in the presence of BIN1 (Fig. 4C). Representative confocal images confirmed the co-localization of ezrin and ezrin-T567D with BIN1 on membranes. We estimated the relative binding of ezrin, wild type or T567D, from the ratio between the intensity of ezrin proteins bound on membranes in the presence of BIN1 or amphiphysin-1 normalized by the intensity of ezrin proteins in the absence of BIN1 or amphiphysin-1. We obtained a ~ 2.5-fold and 1.5-fold increase in the relative membrane binding of ezrin and ezrin-T567D, respectively, in the presence of BIN1 and $PI(4,5)P_2$ (Fig. 4C).

In agreement with the results in Fig. 3A, amphiphysin-1 did not affect ezrin binding on membranes.

To further understand the interplay between BIN1 and ezrin, we investigated the effect of BIN1 knock-down on the established roles of ezrin: cell migration and cell cortex mechanics. Phosphorylated ezrin has been recently associated with increased cell migration (Zhang et al., 2020a). We compared the migration of BIN1 knock-down cells to that of control C2C12 cells. Analysis of mono-dimensional single-cell trajectories (Fig. S3C) showed that BIN1 depletion led to a change in cellular motion, as indicated by the different mean square displacement (MSD) of individual cells over a given time interval (Lag-Time) (Fig. 4E). The observed differences in cellular motility resulted from a significant gain in the migration persistence, whereas it did not modify the mean speed (Fig. S3D). As a central protein linking the actin cytoskeleton to the inner leaflet of the plasma membrane, ezrin is also an important regulator of the cell cortex mechanics (Diz-Muñoz et al., 2010; Sens and Plastino, 2015; Zhang et al., 2020a). We observed using time-lapse phase-contrast videomicroscopy that migrating BIN1-depleted cells form long retraction fibers alike to membrane tethers (Fig. 4F), suggesting a potential role of the BIN1-ezrin association in regulating membrane-to-cortex attachments. We thus investigated the force required to form membrane tethers on myoblasts. To this end, we used atomic force microscopy (AFM) cantilevers coated with poly-L-lysine (Diz-Muñoz et al., 2010) to pull membrane tethers from the plasma membrane of control and BIN1 knock-down C2C12 cells (Fig. 4G). We measured the static tether force, f_0, which is required to hold a membrane tether at a constant height. This force depends on the bending stiffness of the membrane (κ), the surface tension (σ), and the energy density of the membrane-to-cortex attachments (W_0) (Sheetz, 2001):

$$f_0 = 2\pi(2(\sigma + W_0)\kappa)^{1/2}$$

In agreement with the presence of tethers behind migrating BIN1 knock-down cells (Fig. 4F), we found that the apparent static tether force is decreased in these cells, showing that BIN1 contributes to the mechanical properties of the cell cortex (Fig. 4G), which could be associated to its effect on phospho-ezrin distribution at the plasma membrane (Fig. 4B).

Altogether, these data indicate that BIN1 regulates the fine tuning of ezrin recruitment to PI(4,5)P_2-containing membranes, and thus cell cortex homeostasis.

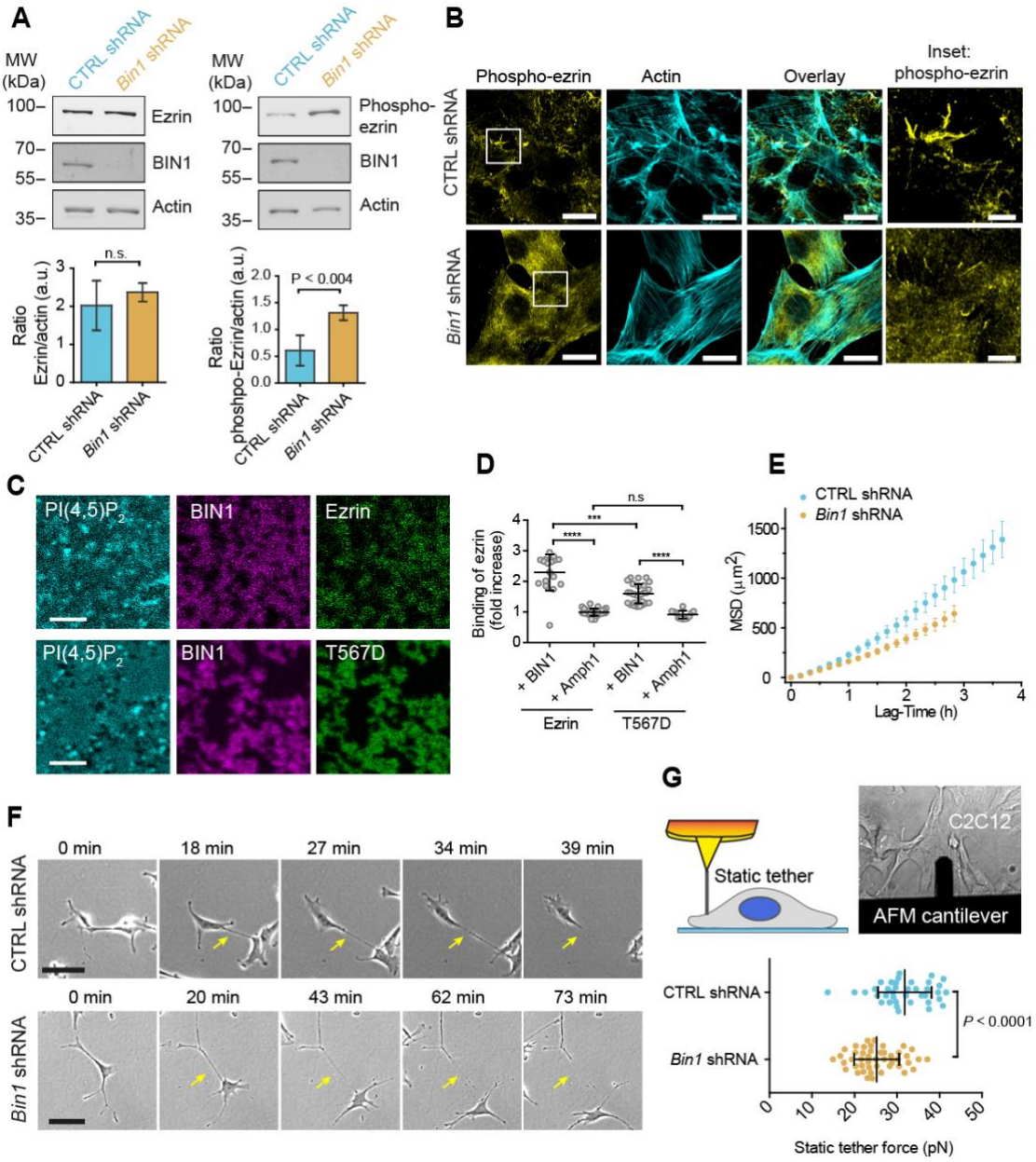

Figure 4. BIN1 regulates the mechanical response of the plasma membrane.

A) Western-blot analysis of the endogenous expression of ezrin and phosphorylated ezrin (phospho-ezrin), BIN1 and actin on cell extracts from CTRL (blue) and BIN1 shRNA (yellow) C2C12 myoblasts, and the corresponding quantification of the signal of each protein normalized by actin. **B)** CTRL and BIN1 shRNA stable C2C12 myoblasts cultured in growth factor-containing medium and stained for endogenous phosphorylated ezrin (phospho-ezrin, yellow) and F-actin (phalloidin, cyan). Inset, high-magnification images showing the localization of endogenous phosphorylated ezrin. Maximum intensity projected airyscan images. Scale bar, 10 μm and 5 μm, respectively. **C)** Still confocal images of the co-localization of recombinant BIN1-Alexa647 (magenta), ezrin or phospho-mimetic ezrin (T567D) tagged with Alexa488 (green) and TopFluor-TMR-PI(4,5)P_2 (cyan) on supported lipid bilayers containing 5% of PI(4,5)P_2. Scale bar: 3 μm. **D)** Fold increase in the binding of recombinant ezrin and T567D on supported lipid bilayers containing 5% PI(4,5)P_2 in the presence of BIN1 or amphiphysin-1 (Amph-1). **E)** Mean square displacement (MSD) in μm^2 for the CTRL (blue) and BIN1 shRNA (yellow) C2C12 cells. **F)** Snapshots of bright field images of CTRL and BIN1 shRNA C2C12 myoblasts cultured in growth factor-containing medium at different time points. Yellow arrow highlights the retraction of retraction fibers formed during cell migration. Scale

bar, 50 μm. **G)** Schematic representation of a plasma membrane tether pulling assay using an AFM cantilever coated with poly-L-lysine on adherent C2C12 cells. Representative bright field image of the corresponding experimental setup. Static tether force (pN) obtained with CTRL (blue) and BIN1 shRNA (yellow) C2C12 myoblasts. t-test: $P < 0.0001$.

Discussion

We unravel here an unexpected role of BIN1 in promoting filopodia-like structure formation in skeletal muscle cells, structures that play a crucial role in myoblast adhesion and fusion in mammalian cells and *Drosophila* (Segal et al., 2016; Zhang et al., 2020b). The sequence of events that can be envisioned for the BIN1/ezrin-mediated formation of filopodia-like protrusions at the myoblast cortex is presented in Fig. 5.

Whereas BIN1 was shown to promote positive membrane curvature (Lee et al., 2002; Picas et al., 2014).), we show here that BIN1 could also regulate the formation of membrane protrusions that have negative membrane curvature. Indeed, BIN1 expression in skeletal muscle cells promotes filopodia-like structure formation, and, reciprocally, its knock-down decreases their density at the cell surface, including at intercellular cell-cell contacts. The generation of these filopodia-like structures by BIN1 requires IRSp53, an I-BAR protein that initiates the formation of filopodia (Lim et al., 2008; Disanza et al., 2013; Prévost et al., 2015) and is implicated in the generation and maintenance of filopodia during the fusion process in *Drosophila* (Segal et al., 2016).

Among the BIN1 partners known to regulate actin remodeling and myoblast fusion are WASP and dynamin (Yamada et al., 2009; Chuang et al., 2019; Zhang et al., 2020b). Notably, WASP also binds the SH3 domain of IRSp53 (Lim et al., 2008). Our proteomic analysis of the BIN1 partners confirmed an association with dynamin and actin, and identified the ERM family proteins. We focused on the BIN1/ezrin interaction and function because ezrin is known to play a crucial role in linking actin to the plasma membrane in different types of membranes protrusions (filopodia, microvilli), where it appears enriched (Osawa et al., 2009) and also to participate in myoblast fusion (Zhang et al., 2022). BIN1 is the only amphiphysin member tested to associate with ezrin. We showed that BIN1 and the phosphorylated active version of ezrin are co-localized at filopodia-like structures (Fig. 3H). How could ezrin be recruited to the cell surface by BIN1? We propose that this could be done through the BIN1-mediated $PI(4,5)P_2$ local enrichment at the plasma membrane during the initial stages of filopodia formation, where the membrane geometry is compatible with the BAR domain of BIN1. Indeed, BIN1 was shown to induce stable $PI(4,5)P_2$ domains that can recruit downstream partners (Picas et al., 2014). The $PI(4,5)P_2$ binding site in the FERM domain of ezrin is

essential for its targeting from the cytosol to the plasma membrane, where a subsequent T567-phospho-dependent unmasking of the F-actin binding domain occurs (Fievet et al., 2004). We have shown that BIN1 enhances ezrin recruitment to PI(4,5)P_2, a phosphoinositide known to be enriched at myoblast fusion sites (Bach et al., 2010; Bothe et al., 2014). In the absence of BIN1, phospho-ezrin is not enriched at filopodia-like membrane protrusions (Fig. 4B). Moreover, the interaction of BIN1 with its downstream partner dynamin is likely to enhance the formation of actin-rich protrusions *via* its multifilament actin-bundling ability required for efficient myoblast fusion (Zhang et al., 2020b). BIN1 is closely connected with F-actin along filopodia-like structures, possibly as a result of its role in promoting the bundling of actin fibers (Fig. 2).

The presence of F-actin-enriched invasive protrusions at the fusion site is a crucial event during myoblast fusion (Sens et al., 2010; Shilagardi et al., 2013). Thus, the formation of PI(4,5)P_2/ezrin specialized domains likely favors the local accumulation of actin filaments to promote filopodia formation. This is in agreement with the described role of ezrin as a major regulator linking the plasma membrane to the cortical actin (Diz-Muñoz et al., 2010; Rouven Brückner et al., 2015) and with studies showing that increased PI(4,5)P_2 concentration recruits more ezrin to the membrane (Braunger et al., 2013; Tsai et al., 2018). BIN1-mediated filopodia-like structures requires IRSp53 and both proteins might work in synergy to increase the binding of ezrin through a PI(4,5)P_2-rich interface, as IRSp53 is expected to enrich PI(4,5)P_2 and ezrin in negatively curved membranes (Prévost et al., 2015; Tsai et al., 2018). Using AFM, we have shown that BIN1 regulates the apparent static tether force (Fig. 4G). The absence of BIN1 would contribute to a disorganization of PI(4,5)P_2 /ezrin at the plasma membrane, and consequently to a loose membrane-to-cortex attachment and a decrease in the formation of filopodia-like structures. Indeed, the long membrane tails in migrating cells that we observed upon BIN1 knock-down would reflect a loosening of membrane-cortex attachments (Fig. 4).

In conclusion, our study suggests a dual function of BIN1 both as a scaffold to recruit proteins, including ezrin, at the cell cortex and as an actin-bundling protein (Fig. 5). We found that BIN1 localizes at the base of filopodia-like structures, a role that increases the actin-membrane cortex tightness, but we also located it in filopodia-like structures, possibly due to its actin bundling properties. The particular function of the stable and long-lived BIN1-mediated filopodia-like structures compared to other types

of filopodia might rely on their suitability to indent neighboring cells, the driving mechanism for myoblast fusion (Vasyutina et al., 2009; Sens et al., 2010; Shilagardi et al., 2013). Finally, we found a tandem role of IRSp53 and BIN1, in filopodia-like structure formation. The association of IRSp53 with antagonistic BAR domain proteins was reported to participate in filopodia formation (Galic et al., 2014; Dobramysl et al., 2021) or assist endocytosis (Bisi et al., 2020) in different cell types and organisms. Why proteins with opposite curvature domains are required to enable distinct remodeling events at the plasma membrane is yet an open question but suggests that the spatio-temporal regulation of these events might be more complex than previously anticipated.

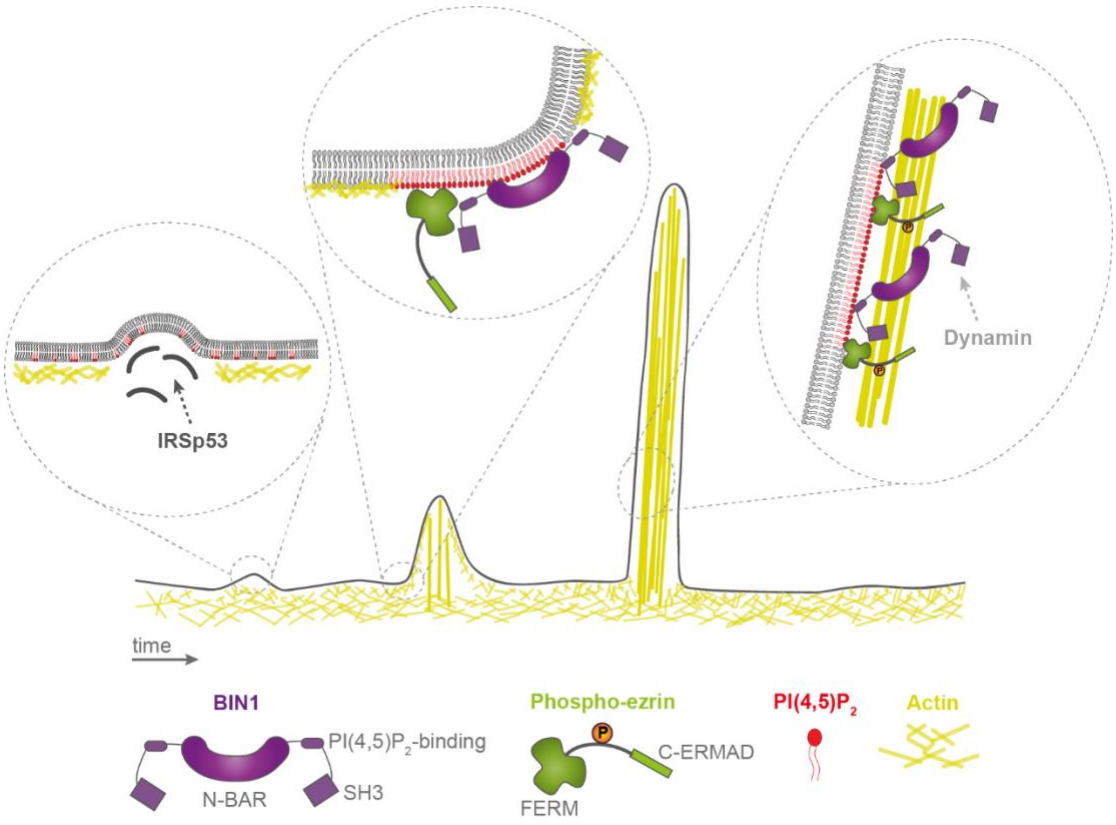

Figure 5. Model of BIN1/ezrin-mediated formation of filopodia-like protrusions at the myoblast membrane. The following steps are shown: 1) formation of BIN1-mediated filopodia-like structures requires an IRSp53-based actin complex, possibly leading to the initial evagination of the plasma membrane (Prévost et al., 2015). Subsequent binding of BIN1 at the plasma membrane might led to $PI(4,5)P_2$ clustering formation (Picas et al., 2014). 2) The $PI(4,5)P_2$ enrichment facilitates the recruitment of ezrin at the cell cortex and the association of its active phosphorylated version (phospho-ezrin) with at filopodia-like protrusions. 3) The membrane remodeling and actin bundling ability of BIN1 promotes filopodia formation in association with phospho-ezrin. At this stage, BIN1 could potentially recruit its downstream partner dynamin and enhance the formation of actin-rich protrusions *via* its multifilament actin-bundling ability required for an efficient myoblast fusion (Zhang et al., 2020b). The different molecular players involved in this process are shown in the legend (BIN1 in magenta, phospho-ezrin in green, actin in yellow, and $PI(4,5)P_2$ in red).

Methods

Reagents

Natural and synthetic phospholipids, including POPS, POPC, POPE and TopFluor-TMR-PI(4,5)P_2 are from Avanti Polar Lipids, Inc. Alexa Fluor 647 and 488 Maleimide labelling kits are from Invitrogen.

The following antibodies were used in this study: monoclonal mouse antibody to BIN1 (clone C99D against exon 17) from Millipore, polyclonal rabbit antibody to IRSp53 (BAIAP2) from Atlas Antibodies (HPA023310), HRP-conjugated beta actin monoclonal antibody from Proteintech (HRP-60008), ezrin antibody from M. Arpin laboratory(Algrain et al., 1993), monoclonal rabbit antibody to phospho-Ezrin (Thr567)/Radixin (Thr564)/Moesin (Thr558) Cell Signaling (Cat. 3726). Atto390 488 phalloidin was from Sigma.

Constructs

pGEX-Sumo vector coding for GST-BIN1 isoform 8 (M-Amphiphysin2) was obtained by Gibson assembly from (Picas et al., 2014). pGEX vectors coding for GST-BIN1 isoform 8 K575X and D151N were obtained as in (Picas et al., 2014). 6xHis-Sumo ezrin and T567D vectors were obtained as in (Tsai et al., 2018). pEGFP-BIN1 D151N, pEGFP-BIN1 K575X were obtained as in (Nicot et al., 2007). pEGFP BIN1 isoform 8 was obtained from P. De Camilli (Yale University, New Haven). pEGFP-BIN1 isoform 9 (N-Amphiphysin2) and pEGFP-Amphiphysin1 were obtained from J. Laporte (Strasbourg). mCherry-ezrin was obtained from (Gautreau et al., 2000) after cloning into pENTR1A Gateway entry vector (Invitrogen) and recombined into mCherry-C1, as described in (Tsai et al., 2018).

Cell culture and transfection

HeLa cells (CCL2 from ATCC) were cultured in DMEM medium (Gibco BRL) supplemented with 10% fetal bovine serum, 100 U/ml penicillin/streptomycin, and 2 mM glutamine. C2C12 mouse myoblasts (ATCC CRL-1772) were grown in DMEM/Ham's F-12 (1:1) supplemented with 10% fetal bovine serum. To induce differentiation, the growth medium was replaced with differentiation medium consisting of DMEM/Ham's F-12 supplemented with 2% fetal calf serum (Hyclone/Perbio Sciences, Brebieres, France). All cells were tested mycoplasma free.

Co-immunoprecipitation, western blot experiments and proteomic assays

To test the interaction between Amphiphysin isoforms and endogenous actin or ERM proteins, HeLa cells (CCL2 from ATCC) were seeded on 50 cm petri dishes overnight. Cells were then transfected for 24 h with either GFP, full-length GFP-BIN1 isoform 8, GFP-BIN1 isoform 9 and GFP-Amphiphysin1 using x-tremGENE9 (Roche). Cells were then trypsinized, washed once in PBS, and incubated on ice for 60 min in a lysis buffer: 25 mM Tris pH 7.5, 50–100 or 200 mM NaCl, and 0.1% NP40. Cells were then centrifuged 10 min at 10,000×g to collect the supernatant. Extracts were processed for co-immunoprecipitation using GFPTrap (Chromotek) following manufacturer's instructions.

To test the interaction of BIN1 and its mutated variants, C2C12 myoblasts were seeded overnight and transfected for 24h with either GFP, full-length GFP-BIN1 isoform 8 WT, K575X and D151N using JetPEI (Ozyme). Co-immunoprecipitation assay was performed as detailed above.

For western-blot experiments cell lysis was performed in 25 mM Tris pH 7.5, 50 mM NaCl, 0.1% NP40, and a protease inhibitor cocktail (Sigma). The following primary antibodies were used: rabbit anti-ezrin (from M. Arpin laboratory (Algrain et al., 1993); 1:1000), mouse anti-actin (Sigma; 1:1000), mouse anti-BIN1 (clone C99D from Millipore; 1:1000), phosphor-ezrin. Secondary Horseradish Peroxidase (HRP)-coupled antibodies were from Jackson Laboratories.

For proteomic analysis, HeLa cells were transiently transfected with either GFP or GFP-BIN1 using X-tremeGENE 9 (Sigma-Aldrich), according to the manufacturer's instructions. Cell lysis and co-immunoprecipitation using GFP-Trap (Chromotek) was performed as described above. Mass spectrometry analysis was performed at the Proteomic platform of Institut Jacques Monod (Paris, France). Positive hits binding to GFP-Bin1 were selected relatively to their corresponding score.

Short interfering RNA (shRNA) stable cell lines

shRNA constructs were engineered on a pSIREN retroviral vector (Clontech). To deplete the endogenous expression of BIN1, the oligonucleotide 5'-GATCCG**CCTGATATCAAGTCGCGCATT**TTCAAGAGA**AATGCGCGACTT GATATCAGG**CTTTTTTACGCGTG-3' was inserted into pSIREN. Bold letters correspond to exons 5/6's junction of mouse *Bin1*. As a control, we used the

oligonucleotide 5'-GTTGCGCCCGCGAATGATATATAATGttcaagagaCATTATATATCATTCGCGGGCGCAAC-3' sequence against luciferase. Hygromycin-resistant HEK293T cells expressing shRNA BIN1 were cultured and cell-free supernatants containing retrovirus were harvested. Infection of C2C12 myoblasts was performed as described previously described (Meriane et al., 2000). C2C12 cells constitutively expressing shRNA BIN1 and CTRL shRNA luciferase were grown in hygromycin.

RNA interference

The siRNA used in this study to IRSp53 was ON-TARGET plus siIRSp53 (BAIAP2) mouse (Horizon Discovery, Cat# J-046696-11) (Rodríguez-Pérez et al., 2021). The siRNA sequence targeting luciferase (CGUACGCGGAAUACUUCGA) was used as a control and was obtained from Sigma. siRNA delivery was performed using Lipofectamine RNAiMAX, according to the manufacturer's instructions.

Time-lapse fluorescence microscopy

C2C12 cells were seeded on FluoroDish (WPI, France) cell culture dishes overnight. Cells were then transfected for 12 h with either GFP-BIN1, D151N or K575X mutants and Lifeact-mCherry; GFP or GFP-BIN1 and its mutated variants and mCherry-ezrin using JetPEI (Ozyme) following the manufacturer's instructions. Live-cell imaging was performed on a Spinning disk microscope based on a CSU-X1 Yokogawa head mounted on an inverted Ti-E Nikon microscope equipped with a motorized XY Stage. Images were acquired through a 60x objective NA 1.4 Plan-Apo objective with a Photometrics Coolsnap HQ2 CCD camera. Optical sectioning was performed using a piezo stage (Mad City Lab). A dual Roper/ Errol laser lounge equipped with 491 and 561 nm laser diodes (50 mW each) and coupled to the spinning disk head through a single fiber was used. Multi-dimensional acquisitions were performed in streaming mode using Metamorph 7 software. Images were collected every second (500 msec exposure) during 60s.

Immunofluorescence microscopy

Fixed cells were obtained after incubation with 4% paraformaldehyde (PFA) for 3 min at room temperature, washed with PBS, incubated with PBS-0.1 M NH_4Cl for 5 min and then washed with PBS. Finally, cells were permeabilized in 0.1% Triton X-100 for

10 min and blocked with 1% BSA during 10 min. Fixed cells were mounted using mowiol mounting agent and visualized using a Leica DMRA and a CoolSnapHQ2 camera, 100x objective NA 1.25 oil Ph 3 CS (HCX PL APO) and analyzed with the Metamorph software. 3D stacks were acquired and deconvolved to build a projection on one plane using Image J.

For myotube imaging, images were acquired on a Zeiss LSM880 Airyscan confocal microscope (MRI facility, Montpellier). Excitations sources used were: 405 nm diode laser, an Argon laser for 488 nm and 514 nm and a Helium/Neon laser for 633 nm. Acquisitions were performed on a 63x/1.4 objective. Multidimensional acquisitions were performed via an Airyscan detector (32-channel GaAsP photomultiplier tube (PMT) array detector).

Images are presented as a z-projection of all planes.

Tether pulling experiments

Tether pulling experiments were performed on a JPK Nanowizard III mounted on an inverted Zeiss wide-field microscope. Olympus Biolevers ($k = 6\ mN \cdot m^{-1}$) were cleaned in acetone for 5 minutes and then plasma-cleaned for 10 min. Then, cantilevers were soaked briefly in 0.1 M of $NaHCO_3$ (pH 9.0), air dried and immersed in 0.01% poly-L-lysin overnight at 4ºC in a humid chamber. Before the measurements, cantilevers were rinsed three times in PBS and mounted on the AFM cantilever holder. The cantilever spring constant was determined by the thermal noise method, as detailed in (Schillers et al., 2017). For the measurement, cells seeded for 24h on FluoroDish cell culture dishes were kept on DMEM-F12 medium at 37ºC and not used longer than 1 h for data acquisition. Static tether force measurements were performed by retracting the cantilever for 6 μm at a speed of 10 $\mu m \cdot s^{-1}$, and the position was kept constant for 30 s. Resulting force–time curves were analyzed using the JPK analysis software.

Protein purification and fluorescent labelling

Human recombinant full-length BIN1 isoform 8, Amphiphysin 1, ezrin wild-type and ezrin T567D were expressed in Rosetta 2 bacteria and purified by affinity chromatography using glutathione Sepharose 4B beads as previously published (Picas et al., 2014; Tsai et al., 2018). Recombinant proteins were labelled by conjugation with

either Alexa Fluor 488 or 647 following maleimide chemistry (Invitrogen), as in (Picas et al., 2014; Tsai et al., 2018).

Muscle actin was purified from rabbit muscle and isolated in monomeric form in G-buffer (5 mM Tris-Cl-, pH 7.8, 0.1 mM CaCl2, 0.2 mM ATP, 1 mM DTT, 0.01% NaN3) as previously described(Spudich and Watt, 1971).

Lipid bilayer experiments

Lipid mixtures consisted of: 60% POPC, 20% POPE, 10-15% POPS and 5-10% PIs. The amount of total negatively charged lipids was kept to 20% for any of the mixtures containing PIs at the expenses of brain-phosphatidylserine. Fluorescent TopFluor-TMR-PI(4,5)P_2 was added to 0.1%.

Supported lipid bilayers were prepared as described in (Braunger et al., 2013). Experiments were performed by injecting 15 µL of buffer (10 mM Tris, pH 7.4, 100 mM NaCl and 0.5 mg·ml^{-1} of casein). Supported lipid bilayers were imaged on a Zeiss LSM880 Airyscan confocal microscope (MRI facility, Montpellier). Excitations sources used were: Argon laser for 488 nm and 514 nm and a Helium/Neon laser for 633 nm. Acquisitions were performed on a 63x/1.4 objective.

F-actin bundling assay

Actin (1 µM, non-labeled) was polymerized 1 hour in a buffer containing 100 mM KCl, 1 mM $MgCl_2$, 0.2 mM EGTA, 0.2 mM ATP, 10 mM DTT, 1 mM DABCO, 5 mM Tris pH 7.5 and 0.01% NaN3 in the presence of BIN1 at different concentrations. Then, 5 µl of the protein mixtures was diluted 20 times (i.e., 50 nM of filamentous actin in the presence of BIN1) in the same buffer supplemented with 0.3% methylcellulose and 660 nM of Alexa Fluor 546-phalloidin. Samples were observed using TIRF microscopy (Eclipse Ti inverted microscope, 100x TIRF objectives, Quantem 512SC camera).

Image processing and analysis

Protein binding was quantified by measuring the mean grey value of still confocal images of either AlexaFluor 488 ezrin, WT or T567D, in the absence of BIN1 or Amphiphysin 1. The obtained average intensity was then used to estimate the fold increase in the binding of ezrin, WT or T567D, in the presence of 0.1 µM of BIN1 or Amphiphysin 1 tagged with AlexaFluor 647. Each data set was performed using the

same supported lipid bilayer preparation and confocal parameters were kept constant between experiments and samples. Mean gray values were measured once the steady-state of protein binding was reached, which was estimated to be ≥ 600 s. Mean gray values were measured using Image J (Schindelin et al., 2012).
To obtain actin fluorescence intensities on a filament or bundles, we manually defined a ROI, a 6 pixel-width line perpendicularly to the filament or bundle. We then obtained the intensity profile of the line in which the x-axis of the profile is the length of the line and the y-axis is the averaged pixel intensity along the width of the line. The actin intensity was the maximum intensity value in the intensity profile.
Filopodia density, morphology and dynamics were analyzed by a custom written program allowing the semi-automatic tracking the Life-actin signal of time-lapse movies using Image J.
Cell tracking was performed using the Manual Tracking plugin on Image J. N ≥ 80 cells per conditions were tracked and analyzed using the R software, as previously reported (Maiuri et al., 2015).

Statistical analyses

Results are shown as a mean ± standard deviation (s.d.). Unless stated otherwise, average values represent at least 3 experimental replicates. Statistical significance was assessed by one-way ANOVA test, unless stated otherwise.

References

Abmayr, S.M., and G.K. Pavlath. 2012. Myoblast fusion: lessons from flies and mice. Development 139(4): 641–656. doi: 10.1242/dev.068353.

Abramovici, H., and S.H. Gee. 2007. Morphological changes and spatial regulation of diacylglycerol kinase-ζ, syntrophins, and Rac1 during myoblast fusion. Cell Motility 64(7): 549–567. doi: 10.1002/cm.20204.

Algrain, M., O. Turunen, A. Vaheri, D. Louvard, and M. Arpin. 1993. Ezrin contains cytoskeleton and membrane binding domains accounting for its proposed role as a membrane-cytoskeletal linker. The Journal of Cell Biology 120(1): 129–139. doi: 10.1083/jcb.120.1.129.

Bach, A.-S., S. Enjalbert, F. Comunale, S. Bodin, N. Vitale, et al. 2010. ADP-Ribosylation Factor 6 Regulates Mammalian Myoblast Fusion through Phospholipase D1 and Phosphatidylinositol 4,5-Bisphosphate Signaling

Pathways (J. Chernoff, editor). MBoC 21(14): 2412–2424. doi: 10.1091/mbc.e09-12-1063.

Bisi, S., S. Marchesi, A. Rizvi, D. Carra, G.V. Beznoussenko, et al. 2020. IRSp53 controls plasma membrane shape and polarized transport at the nascent lumen in epithelial tubules. Nat Commun 11(1): 3516. doi: 10.1038/s41467-020-17091-x.

Bothe, I., S. Deng, and M. Baylies. 2014. PI(4,5)P2 regulates myoblast fusion through Arp2/3 regulator localization at the fusion site. Development 141(11): 2289–2301. doi: 10.1242/dev.100743.

Braunger, J.A., C. Kramer, D. Morick, and C. Steinem. 2013. Solid Supported Membranes Doped with PIP $_2$: Influence of Ionic Strength and pH on Bilayer Formation and Membrane Organization. Langmuir 29(46): 14204–14213. doi: 10.1021/la402646k.

Chen, E.H. 2011. Invasive Podosomes and Myoblast Fusion. Current Topics in Membranes. Elsevier. p. 235–258

Chuang, M.-C., S.-S. Lin, R.L. Ohniwa, G.-H. Lee, Y.-A. Su, et al. 2019. Tks5 and Dynamin-2 enhance actin bundle rigidity in invadosomes to promote myoblast fusion. Journal of Cell Biology 218(5): 1670–1685. doi: 10.1083/jcb.201809161.

D'Alessandro, M., K. Hnia, V. Gache, C. Koch, C. Gavriilidis, et al. 2015. Amphiphysin 2 Orchestrates Nucleus Positioning and Shape by Linking the Nuclear Envelope to the Actin and Microtubule Cytoskeleton. Developmental Cell 35(2): 186–198. doi: 10.1016/j.devcel.2015.09.018.

Disanza, A., S. Bisi, M. Winterhoff, F. Milanesi, D.S. Ushakov, et al. 2013. CDC42 switches IRSp53 from inhibition of actin growth to elongation by clustering of VASP. EMBO J 32(20): 2735–2750. doi: 10.1038/emboj.2013.208.

Diz-Muñoz, A., M. Krieg, M. Bergert, I. Ibarlucea-Benitez, D.J. Muller, et al. 2010. Control of Directed Cell Migration In Vivo by Membrane-to-Cortex Attachment (W.A. Harris, editor). PLoS Biol 8(11): e1000544. doi: 10.1371/journal.pbio.1000544.

Dobramysl, U., I.K. Jarsch, Y. Inoue, H. Shimo, B. Richier, et al. 2021. Stochastic combinations of actin regulatory proteins are sufficient to drive filopodia formation. Journal of Cell Biology 220(4): e202003052. doi: 10.1083/jcb.202003052.

Dräger, N.M., E. Nachman, M. Winterhoff, S. Brühmann, P. Shah, et al. 2017. Bin1 directly remodels actin dynamics through its BAR domain. EMBO Rep. 18(11): 2051–2066. doi: 10.15252/embr.201744137.

Falcone, S., W. Roman, K. Hnia, V. Gache, N. Didier, et al. 2014. N-WASP is required for Amphiphysin-2/BIN1-dependent nuclear positioning and triad organization in skeletal muscle and is involved in the pathophysiology of centronuclear

myopathy. EMBO Molecular Medicine 6(11): 1455–1475. doi: 10.15252/emmm.201404436.

Fernando, P., J.S. Sandoz, W. Ding, Y. de Repentigny, S. Brunette, et al. 2009. Bin1 Src Homology 3 Domain Acts as a Scaffold for Myofiber Sarcomere Assembly. J. Biol. Chem. 284(40): 27674–27686. doi: 10.1074/jbc.M109.029538.

Fievet, B.T., A. Gautreau, C. Roy, L. Del Maestro, P. Mangeat, et al. 2004. Phosphoinositide binding and phosphorylation act sequentially in the activation mechanism of ezrin. J Cell Biol 164(5): 653–659. doi: 10.1083/jcb.200307032.

Fugier, C., A.F. Klein, C. Hammer, S. Vassilopoulos, Y. Ivarsson, et al. 2011. Misregulated alternative splicing of BIN1 is associated with T tubule alterations and muscle weakness in myotonic dystrophy. Nat Med 17(6): 720–725. doi: 10.1038/nm.2374.

Galic, M., F.-C. Tsai, S.R. Collins, M. Matis, S. Bandara, et al. 2014. Dynamic recruitment of the curvature-sensitive protein ArhGAP44 to nanoscale membrane deformations limits exploratory filopodia initiation in neurons. eLife 3: e03116. doi: 10.7554/eLife.03116.

Gautreau, A., D. Louvard, and M. Arpin. 2000. Morphogenic Effects of Ezrin Require a Phosphorylation-Induced Transition from Oligomers to Monomers at the Plasma Membrane. J Cell Biol 150(1): 193–204. doi: 10.1083/jcb.150.1.193.

Kim, J.H., Y. Ren, W.P. Ng, S. Li, S. Son, et al. 2015. Mechanical Tension Drives Cell Membrane Fusion. Developmental Cell 32(5): 561–573. doi: 10.1016/j.devcel.2015.01.005.

Kojima, C., A. Hashimoto, I. Yabuta, M. Hirose, S. Hashimoto, et al. 2004. Regulation of Bin1 SH3 domain binding by phosphoinositides. EMBO J 23(22): 4413–4422. doi: 10.1038/sj.emboj.7600442.

Lee, E., M. Marcucci, L. Daniell, M. Pypaert, O.A. Weisz, et al. 2002. Amphiphysin 2 (Bin1) and T-Tubule Biogenesis in Muscle. 297: 5.

Lim, K.B., W. Bu, W.I. Goh, E. Koh, S.H. Ong, et al. 2008. The Cdc42 Effector IRSp53 Generates Filopodia by Coupling Membrane Protrusion with Actin Dynamics. Journal of Biological Chemistry 283(29): 20454–20472. doi: 10.1074/jbc.M710185200.

Maiuri, P., J.-F. Rupprecht, S. Wieser, V. Ruprecht, O. Bénichou, et al. 2015. Actin Flows Mediate a Universal Coupling between Cell Speed and Cell Persistence. Cell 161(2): 374–386. doi: 10.1016/j.cell.2015.01.056.

McMahon, H.T., and E. Boucrot. 2011. Molecular mechanism and physiological functions of clathrin-mediated endocytosis. Nat Rev Mol Cell Biol 12(8): 517–533. doi: 10.1038/nrm3151.

Meriane, M., P. Roux, M. Primig, P. Fort, and C. Gauthier-Rouvière. 2000. Critical Activities of Rac1 and Cdc42Hs in Skeletal Myogenesis: Antagonistic Effects

of JNK and p38 Pathways (P.T. Matsudaira, editor). MBoC 11(8): 2513–2528. doi: 10.1091/mbc.11.8.2513.

Nicot, A.-S., A. Toussaint, V. Tosch, C. Kretz, C. Wallgren-Pettersson, et al. 2007. Mutations in amphiphysin 2 (BIN1) disrupt interaction with dynamin 2 and cause autosomal recessive centronuclear myopathy. Nat Genet 39(9): 1134–1139. doi: 10.1038/ng2086.

Osawa, H., C.A. Smith, Y.S. Ra, P. Kongkham, and J.T. Rutka. 2009. The role of the membrane cytoskeleton cross-linker ezrin in medulloblastoma cells. Neuro-Oncology 11(4): 381–393. doi: 10.1215/15228517-2008-110.

Picas, L., J. Viaud, K. Schauer, S. Vanni, K. Hnia, et al. 2014. BIN1/M-Amphiphysin2 induces clustering of phosphoinositides to recruit its downstream partner dynamin. Nat Commun 5(1): 5647. doi: 10.1038/ncomms6647.

Prévost, C., H. Zhao, J. Manzi, E. Lemichez, P. Lappalainen, et al. 2015. IRSp53 senses negative membrane curvature and phase separates along membrane tubules. Nat Commun 6(1): 8529. doi: 10.1038/ncomms9529.

Prokic, I., B.S. Cowling, C. Kutchukian, C. Kretz, H. Tasfaout, et al. 2020. Differential physiological roles for BIN1 isoforms in skeletal muscle development, function and regeneration. Dis. Model. Mech. 13(11): dmm044354. doi: 10.1242/dmm.044354.

Prokic, I., B.S. Cowling, and J. Laporte. 2014. Amphiphysin 2 (BIN1) in physiology and diseases. J Mol Med 92(5): 453–463. doi: 10.1007/s00109-014-1138-1.

Randrianarison-Huetz, V., A. Papaefthymiou, G. Herledan, C. Noviello, U. Faradova, et al. 2018. Srf controls satellite cell fusion through the maintenance of actin architecture. Journal of Cell Biology 217(2): 685–700. doi: 10.1083/jcb.201705130.

Rodríguez-Pérez, F., A.G. Manford, A. Pogson, A.J. Ingersoll, B. Martínez-González, et al. 2021. Ubiquitin-dependent remodeling of the actin cytoskeleton drives cell fusion. Developmental Cell 56(5): 588-601.e9. doi: 10.1016/j.devcel.2021.01.016.

Rouven Brückner, B., A. Pietuch, S. Nehls, J. Rother, and A. Janshoff. 2015. Ezrin is a Major Regulator of Membrane Tension in Epithelial Cells. Sci Rep 5(1): 14700. doi: 10.1038/srep14700.

Royer, B., K. Hnia, C. Gavriilidis, H. Tronchère, V. Tosch, et al. 2013. The myotubularin–amphiphysin 2 complex in membrane tubulation and centronuclear myopathies. EMBO Rep 14(10): 907–915. doi: 10.1038/embor.2013.119.

Schindelin, J., I. Arganda-Carreras, E. Frise, V. Kaynig, M. Longair, et al. 2012. Fiji: an open-source platform for biological-image analysis. Nat Methods 9(7): 676–682. doi: 10.1038/nmeth.2019.

Scita, G., S. Confalonieri, P. Lappalainen, and S. Suetsugu. 2008. IRSp53: crossing the road of membrane and actin dynamics in the formation of membrane protrusions. Trends in Cell Biology 18(2): 52–60. doi: 10.1016/j.tcb.2007.12.002.

Segal, D., N. Dhanyasi, E.D. Schejter, and B.-Z. Shilo. 2016. Adhesion and Fusion of Muscle Cells Are Promoted by Filopodia. Developmental Cell 38(3): 291–304. doi: 10.1016/j.devcel.2016.07.010.

Senju, Y., M. Kalimeri, E.V. Koskela, P. Somerharju, H. Zhao, et al. 2017. Mechanistic principles underlying regulation of the actin cytoskeleton by phosphoinositides. Proceedings of the National Academy of Sciences 114(43): E8977–E8986. doi: 10.1073/pnas.1705032114.

Senju, Y., and P. Lappalainen. 2019. Regulation of actin dynamics by PI(4,5)P2 in cell migration and endocytosis. Current Opinion in Cell Biology 56: 7–13. doi: 10.1016/j.ceb.2018.08.003.

Sens, P., and J. Plastino. 2015. Membrane tension and cytoskeleton organization in cell motility. J. Phys.: Condens. Matter 27(27): 273103. doi: 10.1088/0953-8984/27/27/273103.

Sens, K.L., S. Zhang, P. Jin, R. Duan, G. Zhang, et al. 2010. An invasive podosome-like structure promotes fusion pore formation during myoblast fusion. Journal of Cell Biology 191(5): 1013–1027. doi: 10.1083/jcb.201006006.

Shabardina, V., C. Kramer, B. Gerdes, J. Braunger, A. Cordes, et al. 2016. Mode of Ezrin-Membrane Interaction as a Function of PIP 2 Binding and Pseudophosphorylation. Biophysical Journal 110(12): 2710–2719. doi: 10.1016/j.bpj.2016.05.009.

Sheetz, M.P. 2001. Cell control by membrane–cytoskeleton adhesion. Nat Rev Mol Cell Biol 2(5): 392–396. doi: 10.1038/35073095.

Shilagardi, K., S. Li, F. Luo, F. Marikar, R. Duan, et al. 2013. Actin-Propelled Invasive Membrane Protrusions Promote Fusogenic Protein Engagement During Cell-Cell Fusion. Science 340(6130): 359–363. doi: 10.1126/science.1234781.

Shin, N.-Y., H. Choi, L. Neff, Y. Wu, H. Saito, et al. 2014a. Dynamin and endocytosis are required for the fusion of osteoclasts and myoblasts. J Cell Biol 207(1): 73–89. doi: 10.1083/jcb.201401137.

Shin, N.-Y., H. Choi, L. Neff, Y. Wu, H. Saito, et al. 2014b. Dynamin and endocytosis are required for the fusion of osteoclasts and myoblasts. Journal of Cell Biology 207(1): 73–89. doi: 10.1083/jcb.201401137.

Simunovic, M., C. Prévost, A. Callan-Jones, and P. Bassereau. 2016. Physical basis of some membrane shaping mechanisms. Phil. Trans. R. Soc. A 374(2072): 20160034. doi: 10.1098/rsta.2016.0034.

Spudich, J.A., and S. Watt. 1971. The Regulation of Rabbit Skeletal Muscle Contraction. Journal of Biological Chemistry 246(15): 4866–4871. doi: 10.1016/S0021-9258(18)62016-2.

Tsai, F.-C., A. Bertin, H. Bousquet, J. Manzi, Y. Senju, et al. 2018. Ezrin enrichment on curved membranes requires a specific conformation or interaction with a curvature-sensitive partner. eLife 7: e37262. doi: 10.7554/eLife.37262.

Vasyutina, E., B. Martarelli, C. Brakebusch, H. Wende, and C. Birchmeier. 2009. The small G-proteins Rac1 and Cdc42 are essential for myoblast fusion in the mouse. Proceedings of the National Academy of Sciences 106(22): 8935–8940. doi: 10.1073/pnas.0902501106.

Vignjevic, D., S. Kojima, Y. Aratyn, O. Danciu, T. Svitkina, et al. 2006. Role of fascin in filopodial protrusion. Journal of Cell Biology 174(6): 863–875. doi: 10.1083/jcb.200603013.

Wechsler-Reya, R.J., K.J. Elliott, and G.C. Prendergast. 1998. A Role for the Putative Tumor Suppressor Bin1 in Muscle Cell Differentiation. Mol. Cell. Biol. 18(1): 566–575. doi: 10.1128/MCB.18.1.566.

Wu, T., Z. Shi, and T. Baumgart. 2014. Mutations in BIN1 Associated with Centronuclear Myopathy Disrupt Membrane Remodeling by Affecting Protein Density and Oligomerization (L. Johannes, editor). PLoS ONE 9(4): e93060. doi: 10.1371/journal.pone.0093060.

Yamada, H., S. Padilla-Parra, S.-J. Park, T. Itoh, M. Chaineau, et al. 2009. Dynamic Interaction of Amphiphysin with N-WASP Regulates Actin Assembly. J. Biol. Chem. 284(49): 34244–34256. doi: 10.1074/jbc.M109.064204.

Zhang, X., L.R. Flores, M.C. Keeling, K. Sliogeryte, and N. Gavara. 2020a. Ezrin Phosphorylation at T567 Modulates Cell Migration, Mechanical Properties, and Cytoskeletal Organization. IJMS 21(2): 435. doi: 10.3390/ijms21020435.

Zhang, R., D.M. Lee, J.R. Jimah, N. Gerassimov, C. Yang, et al. 2020b. Dynamin regulates the dynamics and mechanical strength of the actin cytoskeleton as a multifilament actin-bundling protein. Nat Cell Biol 22(6): 674–688. doi: 10.1038/s41556-020-0519-7.

Zhang, R., Y. Wang, Y. Liu, X. Bao, W. Xu, et al. 2022. Ezrin regulated myoblast differentiation/fusion and muscle fiber specialization through PKA-NFAT-MyoD/MEF2csignalling pathway. https://www.researchsquare.com/article/rs-136524/v1 (accessed 23 February 2022).

Acknowledgements

The authors thank J. Viaud for kindly providing the PH-PLCd-Alexa647 probe. We thank C. Le Clainche (Institute for Integrative Biology of the Cell, Gif-sur-Yvette, France) for providing actin and B. Cowling for the design of BIN1 shRNA constructs. We also thank C. Cazevieille for assistance in TEM and J. Mateos-Langerak in SIM OMX imaging. The authors also thank P. Sens for scientific discussions. The authors acknowledge the Nikon Imaging Center at Institut Curie-CNRS, the imaging facility MRI, the PICT-IBiSA, members of the national infrastructure France-BioImaging infrastructure supported by the French National Research Agency (ANR10-INBS-04). L.P. acknowledges the ATIP-Avenir program (AO-2016) for financial support. This project was also supported by grants from the Agence Nationale de la Recherche (ANR) (ANR-13-BSV2-0004-01), the Labex Cell(n)Scale (N° ANR-10- LBX-0038) part of the IDEX PSL (N° ANR-10-IDEX-0001-02 PSL), the Association Française contre les Myopathies (15352), the CNRS, the INSERM, the University of Montpellier, University of Strasbourg, the College de France and the Institut Curie.

Author contributions

Conceptualization of the study: L.P., B.G., C. G-R. and S.M-L. Performed experiments and data analysis: L.P., F.C., C.A-A, H.B., F-C-T., J. P., F.R., P.M., S.B., A-S. N, and S.M-L. Supervision: L.P., J.L., P.B., B.G., C.G-R., and S.M-L. Writing: L.P., C.G-R. and S.M-L with inputs from all authors.

SUPPLEMENTARY INFORMATION

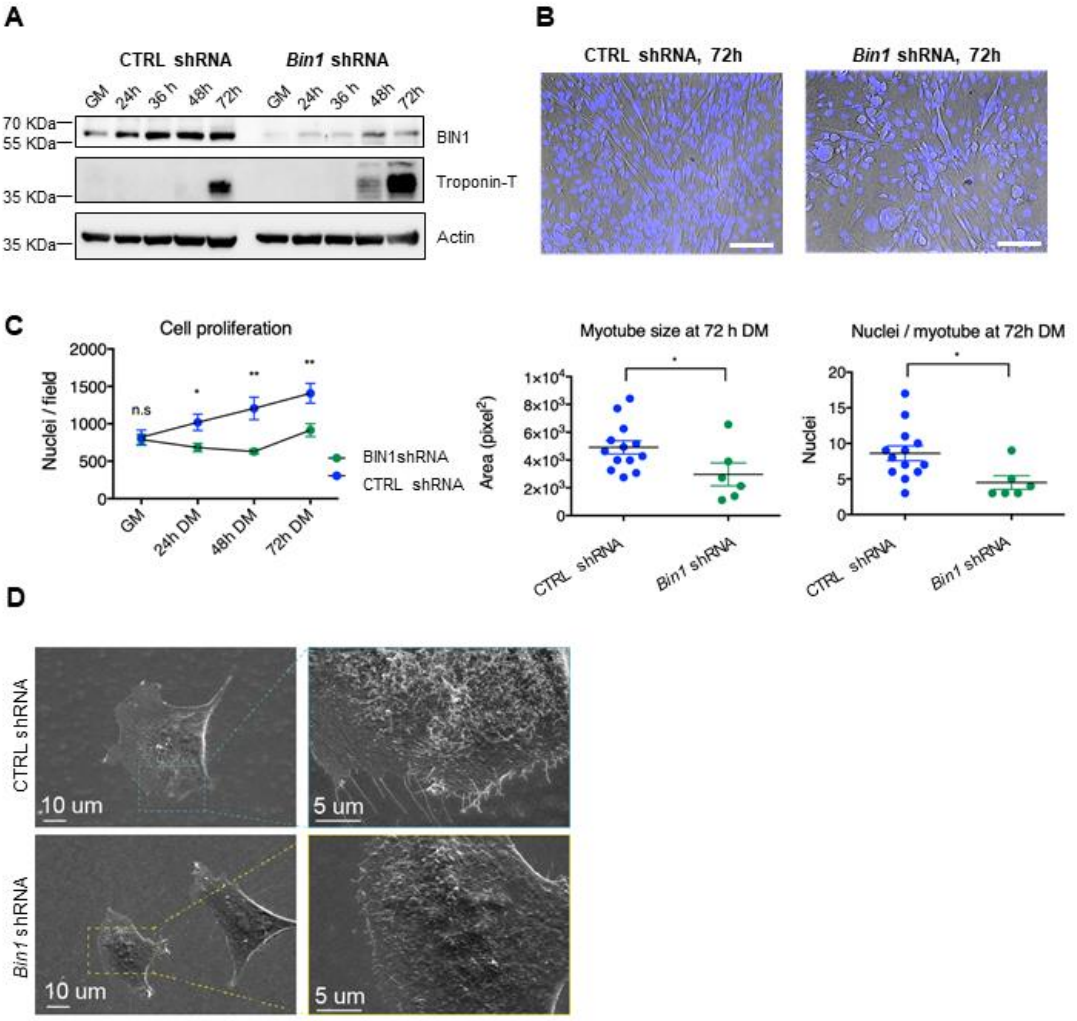

Figure S1. A, Western-blot analysis of the endogenous expression of actin, BIN1 and Troponin-T in CTRL (i.e. Luciferase) shRNA and *Bin1* shRNA stable C2C12 myoblast cell lines during myoblast differentiation: GM (growth medium, undifferentiated) and grown in differentiation medium (DM) at 24h, 36h, 48h and 72h. **B,** Representative wide-field images of C2C12 myoblasts CTRL shRNA or *Bin1* shRNA and the nuclei staining (Hoechst, in blue). Scale bar = 100 µm. **C,** From wide-field images of the C2C12 CTRL shRNA (blue) and *Bin1* shRNA (green), we calculated the cellular proliferation (measured the number of nuclei per field of image), the size of myotubes (in pixels^2) and the number of nuclei per myotube. t-test: n.s > 0.1, * P < 0.1. ** P < 0.01. **D,** Representative SEM images displaying the plasma membrane organization of isolated C2C12 myoblasts expressing either *Bin1* shRNA or CTRL shRNA (*luciferase*) under proliferative conditions.

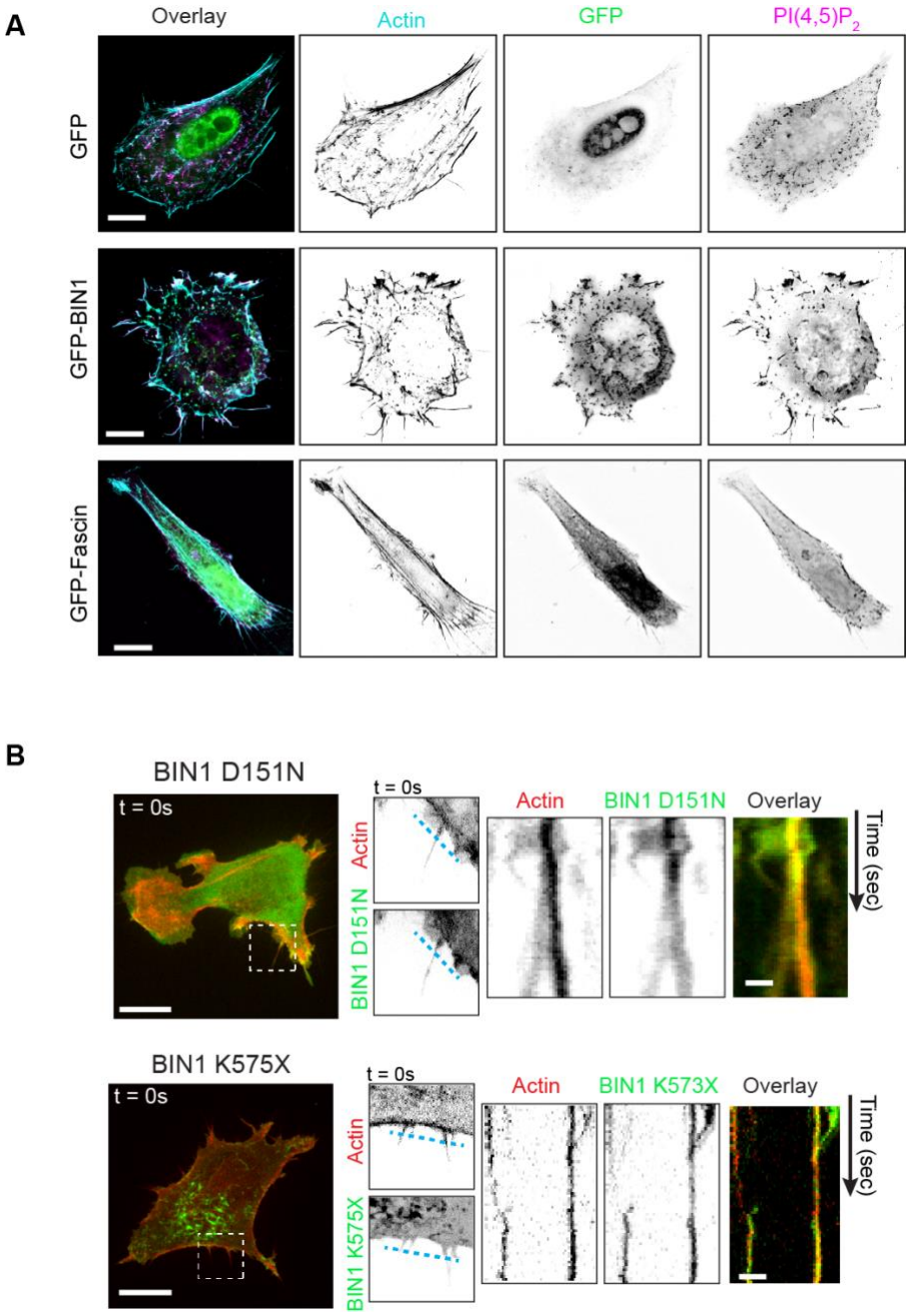

Figure S2. A, Representative images of C2C12 cells transfected with either GFP, GFP-BIN1 or GFP-Fascin and stained for endogenous PI(4,5)P_2 (PH-PLCd-Alexa647, magenta) and F-actin (phalloidin, cyan). Scale bar, 10 µm. **B**, Representative spinning disk live cell imaging (500 ms, 120s) of C2C12 myoblasts co-transfected with mCherry-Lifeact and either GFP-BIN1 D151N or GFP-BIN1 K575X at t = 0s. Kymograph analysis along the blue dashed lines performed on the magnified regions at the cell periphery from each corresponding image**.** Scale bar, 10 µm. Scale bar in kymographs, 1 µm.

A

	Score	
	GFP	**GFP-BIN1**
BIN1		1519
Dynamin-1		207
Dynamin-2		159
Ezrin	33	191
Actin	96	218

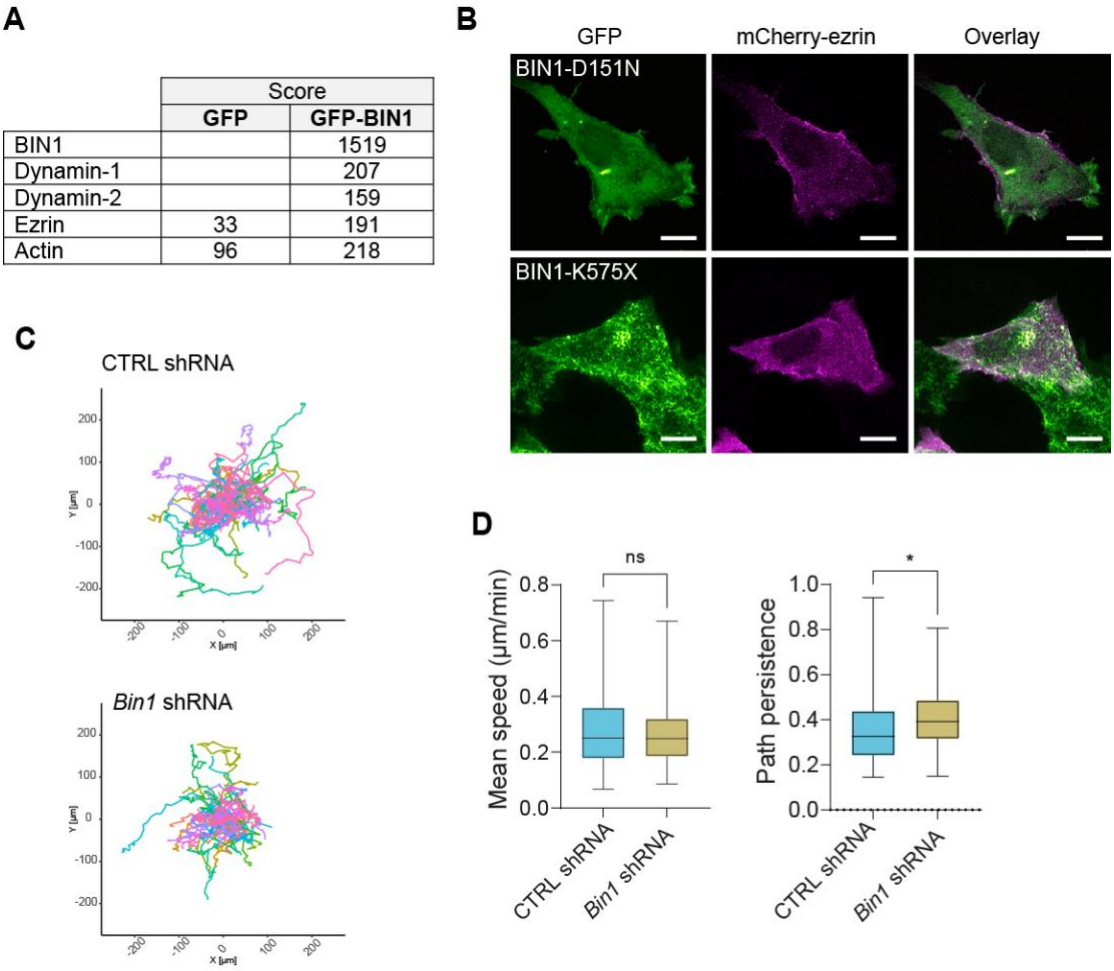

Figure S3. A) Identification of some binding partners of GFP-BIN1 using proteomic analysis. GFP alone was used as a negative control. Only Mascott Scores superior to 50 were considered as positive hits. **B,** Representative time projection of spinning disk movies (500 ms, 120s) of C2C12 myoblasts co-expressing mCherry-ezrin (magenta) and either GFP-BIN1 D151N or GFP-BIN1 K575X (green). Scale bar, 10 µm. **C,** Mono-dimensional single cell trajectories in time. **D,** Distribution of the mean speed and path persistence for the CTRL (cyan) and BIN1 shRNA (yellow) conditions.